Expansion of ring-shaped supracellular contractile cables induces epithelial sheet folding

Fu-Lai Wen*

International Center for Wound Repair and Regeneration, National Cheng Kung University, Tainan 70101, Taiwan and RIKEN Center for Biosystems Dynamics Research, Kobe 650-0047, Japan

(Received 8 June 2022; accepted 5 October 2022; published 5 December 2022)

The folding of epithelial cell sheets is a fundamental process that sculpts developing tissues and organs into their proper shapes required for normal physiological functions. In the absence of detailed biochemical regulations, the epithelial sheet folding may simply proceed through buckling due to mechanical compression arising extrinsically from the surroundings or intrinsically within the sheets. Previous studies hypothesized that the formation of an expanding supracellular actomyosin ring within epithelial sheets could result in compression that ultimately leads to epithelial folding during tracheal development in the *Drosophila* (fruit fly) embryo. However, the exact mechanism by which the formation of epithelial folds is coordinated by the ring expansion remains unclear. Using a vertex-based mechanical model, here I systematically study the dependence of epithelial fold formation on the physical properties of expanding supracellular contractile rings. The simulations show that depending on the contractile strength, epithelial cell sheets can undergo distinct patterns of folding during ring expansion. The formation of folds in particular is robust against fluctuations in the ring properties such as ring numbers and tensions. These findings provide a systematic view to understand how the expansion of supracellular contractile rings in epithelial sheets mediates epithelial folding morphogenesis.

DOI: 10.1103/PhysRevE.106.064403

I. INTRODUCTION

Early embryos are composed of a single layer of epithelial cells. During development, the simple epithelial cell sheet folds into a complex but precise structure that leads to the formation of various tissues and organs such as neural tubes, optic cups, and guts [1,2]. These folding events require highly coordinated processes of cell shape changes, contact rearrangements, and cell divisions, producing the exquisite morphology necessary for the normal functions of tissues and organs [3,4]. Thus, understanding epithelial sheet folding is a key to uncovering the details of complex developmental processes and improving our ability to treat diseases caused by abnormal epithelial morphology.

The genetic and molecular mechanisms underlying epithelial fold formation have been widely studied in the past decades [5,6]. In particular, the regulation of the cytoskeleton in epithelial cells, such as the reorganization of actomyosin networks, was shown to play a central role in mediating a variety of epithelial folding events [7–9]. While many studies have focused on clarifying the chemical machineries behind the epithelial folding process, increased attention is paid to deciphering how mechanical forces generated by the chemical machineries sculpt epithelial fold morphology [10–13].

Previous studies on the morphological development of brains, lungs, and intestines suggested that epithelial cell sheets could establish a regular folded structure through buckling due to mechanical compression [14,15]. In addition to arising extrinsically from the surrounding physical environment, the compressive stress can also be generated intrinsically, for example, by a supracellular contractile actin cable which displays a high concentration of the motor protein myosin (i.e., the actomyosin cable) [16,17]. In many biological contexts, the boundary at which the sheet is being compressed remains static, while the formation of folds occurs when the compressive strength exceeds a certain threshold level. As a result, an inward or outward folded structure forms with equal probability, showing a bifurcation dependent on the compressive strength. Therefore, as a measure of resistance to buckling under compression by a ring-shaped supracellular contractile cable [see Fig. 1(a)], the critical tension Γ^* denotes the minimal tension required for the cable to initiate the sheet folding process [Fig. 1(b)]. Besides the dependence on the physical properties (e.g., geometry and mechanics) of the cell sheet, as proposed by the classical Euler buckling theory [18], the level of Γ^* could also be modulated by the cable property itself. In particular, in contrast to the canonical buckling instability that is induced by the increment of compressive strength (i.e., the cable tension), the critical tension Γ^* could be adjusted due to geometrical changes of the contractile cable, thereby leading to a buckling instability without an elevation of the cable tension. Such a possibility to induce buckling instability is suggested by the recent observation of epithelial invagination in the *Drosophila* tracheal development, where the contractile tension of a supracellular actomyosin cable remains approximately constant during expansion of the cable, while epithelial sheets form a folded structure when the expanding cable grows up to a certain size [19] [see also the schematic illustration in Fig. 1(c)]. Even though a novel buckling instability may underlie *Drosophila* tracheal invagination, many intriguing questions remain unanswered including whether and how the buckling threshold (i.e., Γ^*) is modulated in response to the cable expansion, how the

*fulai@gs.ncku.edu.tw

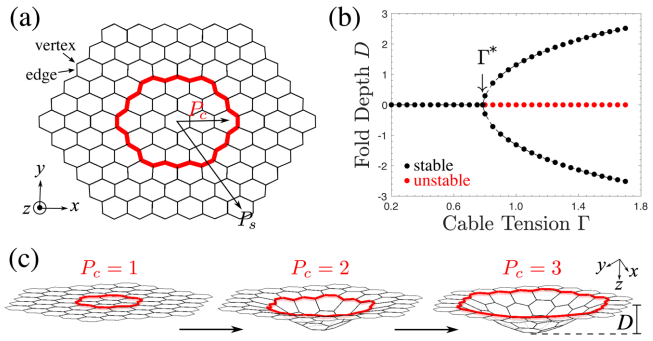

FIG. 1. The formation of epithelial folds coordinated by an expanding circular contractile cable. (a) Schematic of the epithelial cell sheet contracted by a supracellular circular cable (red thick line). The parameters P_c and P_s denote the sizes (number of cell layers) of the cable and the sheet, respectively. (b) A typical bifurcation diagram for the model cell sheet under contraction of a fixed-sized cable. Fold formation occurs when the contractile tension exceeds a certain threshold value Γ^*, where the positive and negative fold depths D represent the inward and the outward folds, respectively. The stable and unstable solutions of epithelial folds are respectively shown in black and red (light gray in grayscale). (c) Snapshots of epithelial fold formation induced by expansion of a contractile cable with fixed tension level. The fold depth D is measured as the difference between the maximum and the minimum z component of the vertex positions.

formation process and the final folded shape depend on the property of the expanding cable, and, more generally, how the distribution pattern of contractile cables influences the formation of folds.

To address the above issues, here a vertex-based mechanical model is presented to systematically study epithelial sheet deformation under the action of ring-shaped supracellular contractile cables. Using computer simulations and numerical analyses, I show that an expansion of contractile cables in epithelial sheets can induce a buckling instability that robustly leads to epithelial folding against fluctuations in the cable properties. In particular, while the elevation of contractile strength is not necessary for fold formation, the qualitative behavior of the folding process is found to depend on the contractile strength. These findings reveal the essential role of expanding supracellular actomyosin cables in epithelial morphogenesis.

II. MODEL

Vertex-based geometric modeling represents a powerful framework for simulating epithelial morphogenesis in various biological contexts [20,21]. Following this modeling approach, a vertex model was developed to simulate contraction-induced shape changes in the apical surface of epithelial cell sheets in three dimensions [Fig. 1(a)], where the apical surface was represented as a hexagonal lattice with vertices and edges. The position of each vertex is changed by the forces which are derived from the derivative of the potential energy function U that accounts for the entire cell sheet mechanics. As a result, each polygonal cell within the lattice deforms to minimize the energy function U, and a stable force-balanced shape is achieved when U reaches a minimum [20,21]. Following previous studies on epithelial shape formation induced by a tissue-scale contractile ring [19,22], here the energy function was constructed by considering the elastic energy of the apical cell area and perimeter, the line tension energy of the cell edges and the circular contractile cables, and the bending energy of the entire apical surface. The energy function U of a tissue comprising N cells is thus formulated as follows,

$$U = K_A \sum_{i=1}^{N} (A_i - A_o)^2 + K_P \sum_{i=1}^{N} P_i^2 + \sum_{e} \Lambda_e \ell_e + \sum_{e \in C} \Lambda_C \ell_e + K_B \sum_{e'} (1 - \hat{\mathbf{n}}_{\mathbf{i}(\mathbf{e}')} \cdot \hat{\mathbf{n}}_{\mathbf{j}(\mathbf{e}')}), \quad (1)$$

where K_A and A_o in the first term are the elastic modulus and the preferred area of the ith polygonal cell with area A_i, respectively, and K_P in the second term is the elastic modulus of its perimeter of length P_i. These two terms take into account the elastic properties of cytoskeletons enriched in the apical surface of an epithelial cell sheet [23]. In the third and fourth terms, Λ_e denotes the line tension at the eth cell edge of length ℓ_e, whereas $\Lambda_C = \Lambda_e(1 + \Gamma)$ with $\Gamma \geqslant 0$ is the line tension of the cell edge that comprises the contractile cable C. The last term serves as a penalty of bending, which sums over all the interior edges e' shared by two adjacent polygonal cells i and j. The surface bending energy is defined by the elastic modulus of bending K_B and the unit normal vectors $\hat{\mathbf{n}}_{\alpha(\mathbf{e}')} = \mathbf{A}_\alpha / A_\alpha$ with $\alpha = i, j$ of the two adjacent polygonal cells [22]. The cell shape features including the cell area A_i, perimeter P_i, edge ℓ_e, and the unit normal vector $\hat{\mathbf{n}}_{\alpha(\mathbf{e}')}$ were calculated from the vertex positions. Thus, for a given set of mechanical properties of the entire cell sheet, the balanced epithelial shape was determined by minimizing the potential U with respect to the vertex positions.

III. RESULTS

A. Dependence of the buckling threshold on the sizes of epithelial cell sheets and contractile cables

During *Drosophila* tracheal development, the number of cells that are involved in epithelial invagination (40–60 cells) is determined by the genetically programed signaling patterns [24,25]. Alterations in the signaling patterns could result in changes in the size of the cell sheets that are expected to undergo folding for the development of tracheal tubes, and therefore lead to an abnormal tube structure. To understand how size variations in epithelial cell sheets as well as in expanding contractile cables influence the folding process, here I sought to determine the dependence of the buckling threshold Γ^* on the cell sheet size P_s and the cable size P_c using the vertex model introduced in Sec. II. To take into account the physical confinement of tracheal cell sheets by the surrounding tissues and the outer eggshell membranes, the movement of the outermost cell layer (i.e., cells at the sheet boundary) were restricted into the xy plane perpendicular to the folding axis [see Fig. 1(a)]. Assuming that each cell in the sheet is identical and has the same mechanical properties (see Table I for a typical choice of parameter values), for given sizes of cell sheet and contractile cable, as well as the cable tension,

TABLE I. Parameter values used for the vertex simulations.

Symbol	Physical meaning	Value	Reference
N	Total number of cells	37–169	[19]
K_A	Elastic modulus of the apical area elasticity	1.0	[19,22,26]
A_o	Preferred apical area	3.0	[19,22,26]
K_P	Elastic modulus of the apical perimeter elasticity	0.1	[19,22,26]
Λ_e	Line tension at the cell edges	0.4641	[19,22,26]
Γ	Normalized line tension of the contractile cables	0.2–1.7	
K_B	Elastic bending modulus of the apical tissue surface	0.1	[19,22]

the potential function U [Eq. (1)] was numerically minimized to obtain the corresponding force-balanced sheet structure. Using the bifurcation diagram analysis shown in Fig. 1(b), the buckling threshold Γ^* for each pair of P_c and P_s was obtained by identifying the balanced sheet structure for the same set of model parameters by varying only the cable tension in the range of $\Gamma =$ 0.2–1.7 (see Fig. 5 in the Appendix for an example). For each Γ, the energy minimization simulations were run in parallel starting from the configuration of a flat cell sheet with random perturbations on each vertex of the sheet. As shown in Figs. 2(a)–2(c), Γ^* is found to be lowered when either the cable size P_c or the cell sheet size P_s increases. In particular, changes in P_c not only shift the level of Γ^* but also alter the relationship of how the fold depth D varies with Γ beyond Γ^* [Fig. 2(d)], where an increase of P_c enhances the deepening of folds in response to the exceeding cable tension $(\Gamma - \Gamma^*)$. In contrast, the relationship remains unchanged when varying P_s [Fig. 2(e)]. These findings suggest that both expansion of the actomyosin cables and increment of the invaginating cell populations could facilitate the formation of epithelial folds during *Drosophila* tracheal development. Notably, the prediction on the cell population effect is in line with the experimental observation on the *rho bnl* double mutants, where tracheal sheets that are composed of a smaller number of invaginating cells were found to exhibit impaired invagination [25]. Furthermore, in contrast to monotonically approaching a certain constant level as P_s increases [Fig. 2(b)], Γ^* first decreases and then slightly increases as P_c grows [Fig. 2(a)]. As revealed by Fig. 6 in the Appendix, such an increment of Γ^* at large P_c may result, at least in part, from the effect of boundary confinement, where restrictions at the sheet boundary impede the contraction of sheets by the cables. Taken together, the simulation results indicate that the contractile cable tension Γ is not the only parameter driving sheet

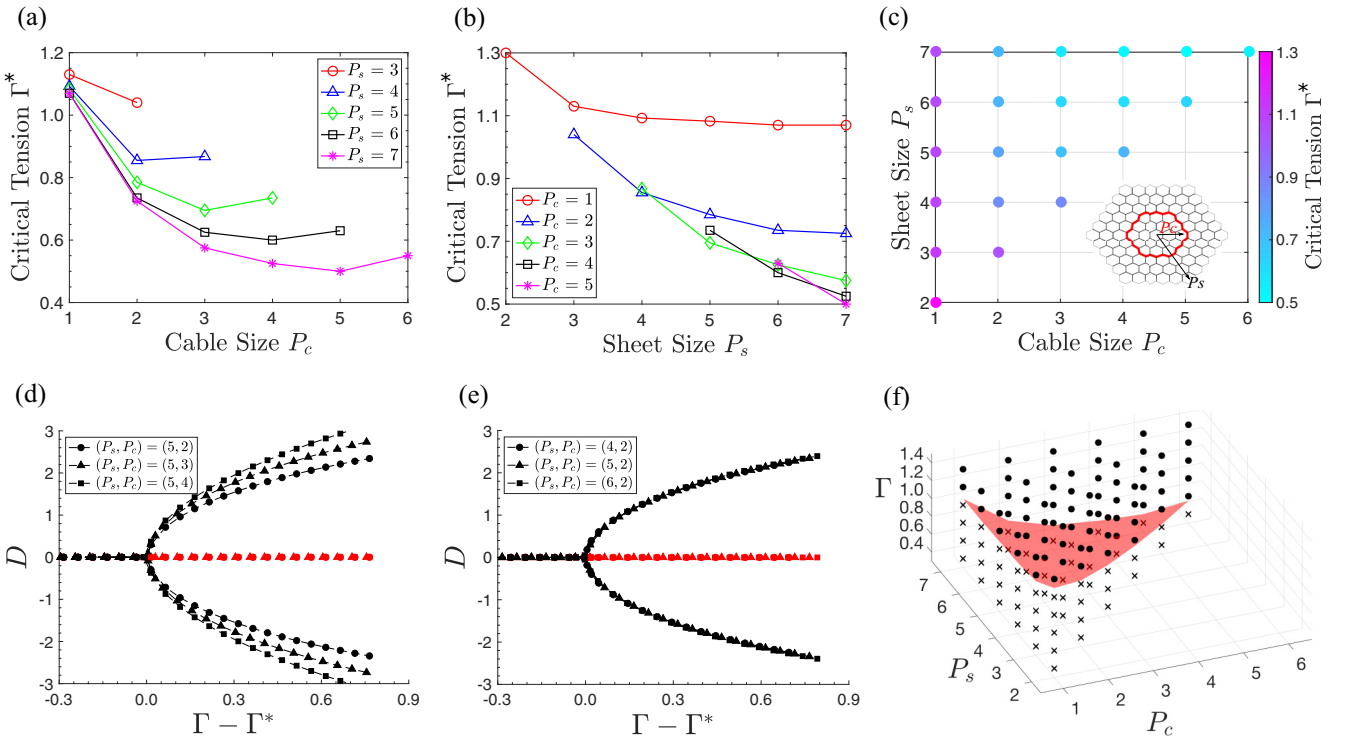

FIG. 2. The influence of the size of (a) contractile cables or (b) cell sheets on the critical tension level Γ^*. (c) Color plot of the critical tension Γ^* as a function of cable size P_c and sheet size P_s. (d) The fold depth D plotted against the relative cable tension $(\Gamma - \Gamma^*)$ for different values of P_c. (e) The dependence of D on $(\Gamma - \Gamma^*)$ for different values of P_s. (f) Phase diagram in the parameter space of P_c, P_s, and Γ showing the formation regions of flat (crosses) and folded (circles) sheets. The surface at the interface was obtained by the Delaunay triangulation of Γ^*.

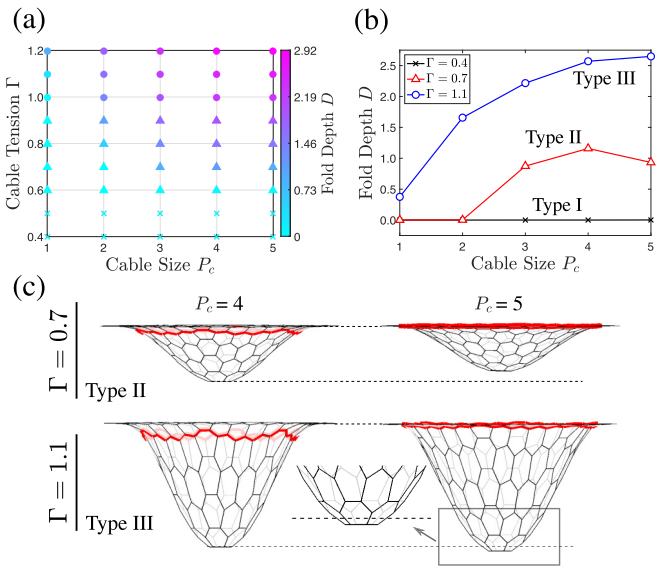

FIG. 3. The tension levels of an expanding circular cable mediate distinct types of fold formation. (a) Color plot of the fold depth D as a function of cable size P_c and cable tension Γ. Symbols mark the distinct types of epithelial fold formation mediated by an expanding contractile cable with a constant tension: type I (×), type II (▲), and type III (●). A representative example showing the different patterns of folding for these three types is given in (b). (c) Variation of the fold depth for type II and type III formation while the cable approaches toward the sheet boundary. The sheet morphology and hereafter were enlarged twofold in the z axis to emphasize the fold depth. The parameters $P_s = 6$ and others shown in Table I were used in the simulations.

folding, but there are two other quantities, the cable size P_c and the cell sheet size P_s, which can induce folding, creating a more complex "phase diagram" of folding that depends on multiple mechanical properties of the system [Fig. 2(f)].

B. Contractile tension of an expanding circular cable regulating different types of folding

Given that the time required to reach mechanical equilibrium (a few tens of seconds [26]) is faster than that for the cable expansion (a few tens of minutes [19]) during *Drosophila* tracheal development, the tracheal invagination can be approximated as a quasistatic process in which the tracheal cell sheets always maintain a force balance during cable expansion. To further study the formation of tracheal folds that occurs concurrently with expanding a circular cable with nearly constant tension, I thus numerically solved the force-balanced cell sheet structure at each step of cable expansion for a given fixed cable tension. As shown in Fig. 3(a), when the cable tension Γ is sufficiently large, the folding of epithelial cell sheets emerges as an increase of the cable size P_c, where the epithelial fold generally becomes deeper as the cable expands. In particular, the variation in the fold depth shows a distinct pattern that depends on the imposed contractile tension. When the cable tension Γ is high, epithelial folds continuously deepen as the cable expands [Figs. 3(b) and 3(c), type III]. For moderate contractile tension, however, a retraction of folds was observed while the cable expands toward the cell sheet boundary [Figs. 3(b) and 3(c), type II]. As illustrated in Fig. 7 in the Appendix, the different types of folding can be understood in terms of the nonmonotonic change of the buckling threshold Γ^* as the cable expands [see Fig. 2(a)] in the near- and far-buckling regimes.

C. Impact of cable arrangement on epithelial fold formation

So far I have shown that without modulation of the contractile strength, a circular cable in epithelial sheets can induce the whole sheet folding by expanding its size due to the lowering of the buckling threshold. Since biological and experimental environments are inherently variable, it is worthwhile to further examine the robustness of such fold formation against fluctuations in the cable properties. In particular, distinct from the switchlike activation of epidermal growth factor receptor activated extracellular-signal regulated kinase (EGFR-ERK) signaling which regulates the formation of a single supracellular actomyosin cable in the *Drosophila* tracheal sheets, a graded activation of the signaling was found to result in the formation of multiple supracellular actomyosin cables [19]. Additionally, the formation of multiple actomyosin cables has also been found in the invagination process of lens placode in chick and mouse embryos [27]. To understand whether and how the multiple contractile cables may mediate epithelial fold formation, here I sought to determine the dependence of epithelial folding on the cable arrangement. Specifically, two contractile cables—the inner cable of smaller size P_{c_1} and the outer cable of larger size P_{c_2}—with the same tensions were considered, and the epithelial fold depth induced by the two cables was systematically studied for all possible arrangements of the cables [Figs. 4(a)–4(c)]. Interestingly, whereas expansion of the inner cable continuously deepens the epithelial cell sheets [Fig. 4(a)], epithelial folds become shallower as the outer cable expands [Fig. 4(b)]. Given that $P_{c_1} < P_{c_2}$, these results thus imply that for a given inner cable size P_{c_1} (or the outer cable size P_{c_2}), the fold depth increases when the absolute difference between the values of P_{c_1} and P_{c_2} is decreased (i.e., the spacing between the two contractile cables is reduced). Particularly, Figs. 4(a) and 4(b) reveal that P_{c_1} seems to be the parameter driving the folding, while P_{c_2} somehow regulates the amplitude of the folding as an auxiliary factor. It would be interesting in the future to investigate whether the fold depth changes can be collapsed onto a single curve that depends on a unified variable that combines both P_{c_1} and P_{c_2}. Furthermore, in comparison to the cell sheets contracted by a single contractile cable, the formation of extra cables in the epithelial sheets results in a deeper fold irrespective of the cable tension [Fig. 4(d), left] and the formation location [Fig. 4(d), right]. Therefore, compared to the expansion of a single contractile cable (where the outer cable forms concurrently with the disassembly of the inner cable), the formation of multiple cables (where the outer cable forms while keeping the inner cable intact) could be more effective for developing epithelial folds.

IV. DISCUSSION

In this study I showed unequivocally that the buckling threshold of epithelial cell sheets under contraction of a supracellular cable generally becomes lowered as the cable size

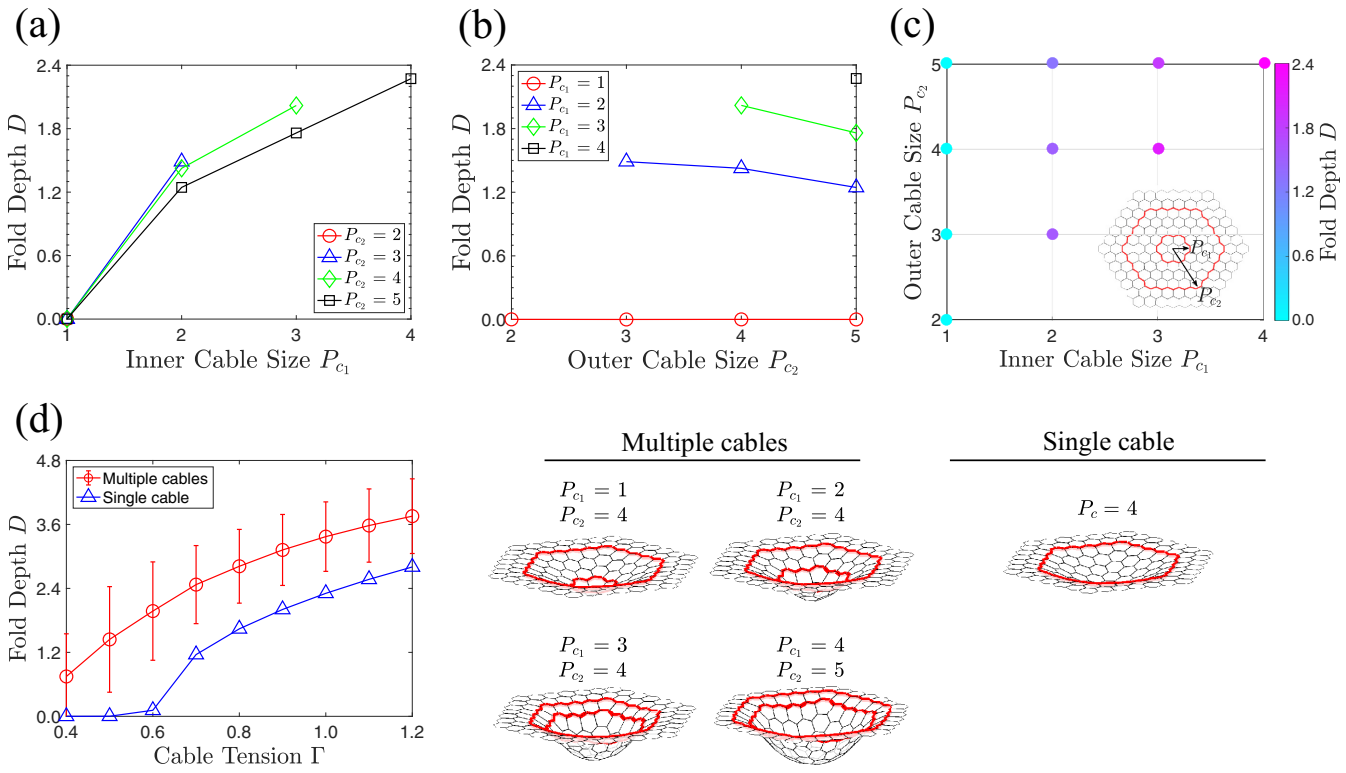

FIG. 4. A typical example illustrating the influence of the size of (a) inner cables or (b) outer cables on the fold depth of epithelial sheets having size $P_s = 6$ and cable tension $\Gamma = 0.5$. (c) Color plot of the fold depth D as a function of inner cable size P_{c_1} and outer cable size P_{c_2}. (d) Left: The epithelial fold depth vs the contractile strength of a single (blue triangle) or multiple cables (red circle with bar), where each data point was averaged over all possible arrangements of multiple cables (see right-hand panel), at which one of the cables has a size of $P_c = 4$ for the comparison of a single cable of the same size, and bars represent the standard deviation of the data samples. Right: Example of representative folds induced by a single or multiple cables. The parameters $\Gamma = 0.8$ and others given in Table I were used in the simulations.

increases (Fig. 2). Through this mechanism, a circular contractile cable in epithelial sheets can fold the entire epithelia simply by expanding its size without the need to modulate the cable tension. The level of cable tension in particular was found to dictate distinct types of folding processes mediated by the cable expansion (Fig. 3). Taking into account the possibility of forming multiple contractile cables during a single cable expansion, I have also studied epithelial sheet deformation induced by two cables. The simulations showed that, compared to a single cable, the formation of an extra cable in the sheets results in a deeper fold irrespective of the cable tension and the formation location (Fig. 4). This suggests that cable expansion-mediated folding is robust against fluctuations in the cable numbers and therefore ensures the reliable formation of epithelial folds. Taken together, these findings underpin the hypothesis that the experimentally observed expansion of a supracellular actomyosin cable within epithelial sheets can induce a buckling instability that drives epithelial invagination during *Drosophila* tracheal development. Using genetic and/or molecular approaches to manipulate actomyosin activity at cell-cell contacts, one may examine the model predictions such as the distinct types of fold formation and their dependence on the cable tension, and evaluate the robustness of invagination morphogenesis in the developing *Drosophila* trachea.

The formation mechanism of supracellular contractile cables was not addressed in the current study. Previous works on *Drosophila* tracheal invagination have found that initially several individual actomyosin segments were formed in epithelial cell sheets. Subsequently, the actomyosin segments were connected and organized into a large-scale round structure through the coordinated rearrangement of cells possibly mediated by the radial expansion of the EGFR-ERK signaling wave emitted from the invagination center [19]. It could be a potentially important issue for future studies to pinpoint the precise mechanism by which the signaling wave coordinates the cell rearrangement to organize the individual actomyosin segments into a large-scale contractile cable.

Buckling instability provides a general mechanism for epithelial folding morphogenesis that occurs in diverse developmental contexts [10]. In this paper, I showed that besides the elevation of the contractile strength to overcome the buckling threshold, a supracellular contractile cable can lower the threshold by expanding its size to initiate the folding process. The multiple routes to achieve folding may enable epithelia to robustly form a folded structure via buckling in a noisy environment. In comparison to a cable of fixed size that relies on a mechanism to maintain the integrity of the cable structure, a varying-size cable requires mechanisms of establishment, maintenance, and remodeling of the

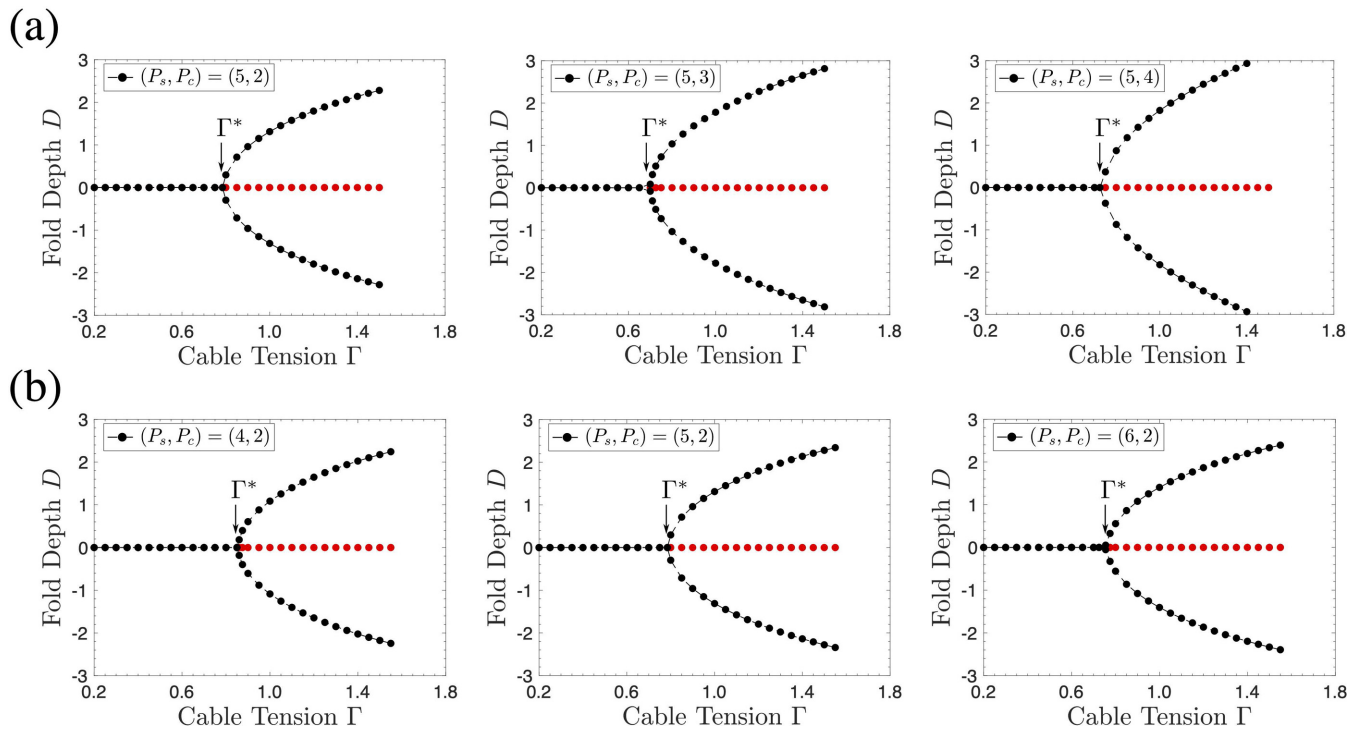

FIG. 5. The fold depth dependence on cable tension changes for different values of P_s and P_c, where the stable and unstable solutions of the fold depth are respectively shown in black and red (light gray in grayscale). The effect of changes in P_c (a) and P_s (b) on how the fold depth D varies with cable tension Γ beyond the threshold value Γ^* is examined in detail in Figs. 2(d) and 2(e).

cable structure. The expanding supracellular actomyosin cable observed during *Drosophila* tracheal invagination serves as an excellent model system to study the versatile mechanisms of the regulation of large-scale actomyosin structures in epithelial sheets. In particular, a combination of regulatory mechanisms determines the expansion dynamics of the supracellular actomyosin cable, and thereby setting a timer for triggering epithelial invagination over the entire developmental period. It is intriguing to investigate how the onset of epithelial morphogenesis depends on the molecular regulations of the supracellular actomyosin cytoskeleton for future studies.

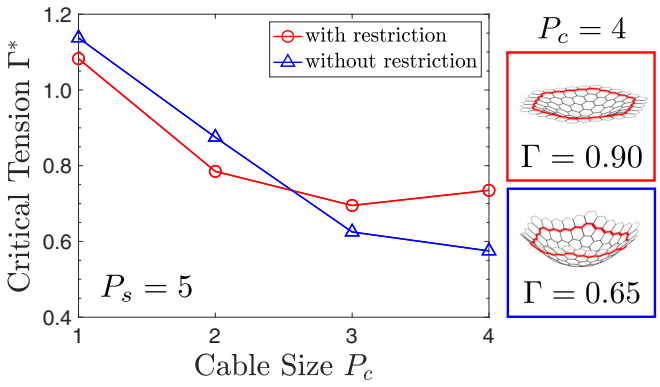

FIG. 6. Spatial confinement on the cell sheet boundary induces a nonmonotonic decrease of Γ^* as P_c increases. Left: The buckling threshold Γ^* as a function of cable size P_c for cell sheets with and without restrictions on their boundaries (see text for details of the restrictions). Right: A representative example of the cell sheets with (top) and without (bottom) boundary restrictions. The parameters $P_s = 5$ and others shown in the figure and Table I were used in the simulations.

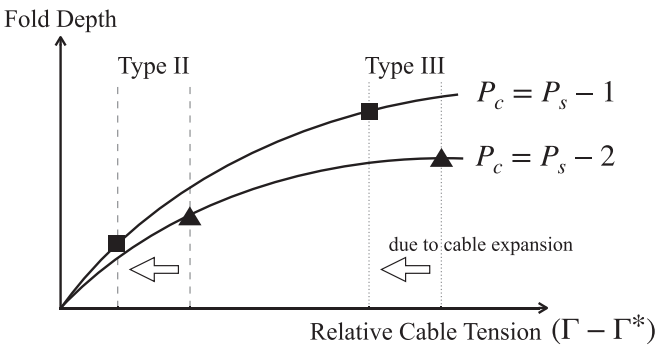

FIG. 7. Schematic illustration of the mechanisms for type II and type III fold formation. The dependence of fold depth on the cable tension Γ for different cable sizes P_c is plotted based on the simulation results shown in Fig. 2(d), where only the upper half of the bifurcation diagram is shown for simplicity. Due to cable expansion, the increment of Γ^* in the late stage of expansion (i.e., $P_c = P_s - 2$ becomes $P_c = P_s - 1$) causes a decrease in the relative cable tension $(\Gamma - \Gamma^*)$. For small cable tension in the near-buckling regime, cable expansion leads the fold depth to become shallower (dashed lines), leading to type II fold formation, whereas the fold depth continuously deepens for large cable tension (dotted lines) showing type III fold formation.

While intracellular cytoskeletons such as actomyosin networks and microtubules are known to play essential roles in the regulation of a single cell shape [28–30], mounting evidence has revealed that the patterning of intracellular cytoskeletons over multiple cells could coordinate individual cell shape changes leading to a tissue-wide morphogenetic process [31]. For example, the organization of actomyosin networks into a supracellular line structure could drive collective cell migration, cell sorting, and embryo segmentation [32–34], whereas a round structure may lead to tissue folding, tissue elongation, and sealing of tissue gaps [33,35]. I envision that the current modeling framework could potentially serve as a generalizable platform that can be modified to study the impact of large-scale geometric patterning of cytoskeletons on epithelial morphogenesis.

ACKNOWLEDGMENT

This work was supported by the National Science and Technology Council of Taiwan under Grant No. NSTC 109-2112-M-006-028-MY3.

APPENDIX

This Appendix provides additional details and Figs. 5–7 for the Results section.

[1] S. F. Gilbert, *Developmental Biology*, 10th ed. (Sinauer Associates, Sunderland, MA, 2013).
[2] D. Fristrom, Tissue Cell **20**, 645 (1988).
[3] S. B. Lemke and C. M. Nelson, Curr. Biol. **31**, R1098 (2021).
[4] E. J. Pearl, J. Li, and J. B. Green, Philos. Trans. R. Soc., B **372**, 20150526 (2017).
[5] J. J. Zartman and S. Y. Shvartsman, Annu. Rev. Chem. Biomol. Eng. **1**, 231 (2010).
[6] C. S. Ko and A. C. Martin, Curr. Top. Dev. Biol. **136**, 141 (2020).
[7] H. Miao and J. T. Blankenship, Development **147**, dev186502 (2020).
[8] K. Röper, Curr. Top. Dev. Biol. **112**, 103 (2015).
[9] N. Gorfinkiel, Dev. Dyn. **245**, 268 (2016).
[10] M. Tozluoğlu and Y. Mao, Philos. Trans. R. Soc., B **375**, 20190564 (2020).
[11] R. Keller and D. Shook, BMC Biol. **9**, 90 (2011).
[12] F.-L. Wen, Y.-C. Wang, and T. Shibata, Biophys. J. **112**, 2683 (2017).
[13] F.-L. Wen, C. W. Kwan, Y.-C. Wang, and T. Shibata, PLoS Comput. Biol. **17**, e1009614 (2021).
[14] C. M. Nelson, J. Biomech. Eng. **138**, 021005 (2016).
[15] K. E. Garcia, C. D. Kroenke, and P. V. Bayly, Philos. Trans. R. Soc., B **373**, 20170321 (2018).
[16] P. Agarwal and R. Zaidel-Bar, Trends Cell Biol. **29**, 150 (2019).
[17] A. C. Martin, Dev. Biol. **341**, 114 (2010).
[18] L. D. Landau, L. P. Pitaevskii, A. M. Kosevich, and E. M. Lifshitz, *Theory of Elasticity*, Course of Theoretical Physics (Elsevier, New York, 1986), Vol. 7, 3rd ed.
[19] Y. Ogura, F.-L. Wen, M. M. Sami, T. Shibata, and S. Hayashi, Dev. Cell **46**, 162 (2018).
[20] A. G. Fletcher, M. Osterfield, R. E. Baker, and S. Y. Shvartsman, Biophys. J. **106**, 2291 (2014).
[21] S. Alt, P. Ganguly, and G. Salbreux, Philos. Trans. R. Soc., B **372**, 20150520 (2017).
[22] N. Murisic, V. Hakim, I. G. Kevrekidis, S. Y. Shvartsman, and B. Audoly, Biophys. J. **109**, 154 (2015).
[23] A. C. Martin and B. Goldstein, Development **141**, 1987 (2014).
[24] S. Manivannan and C. M. Nelson, Stem Cell Res. Ther. **3**, 42 (2012).
[25] T. Kondo and S. Hayashi, eLife **8**, e45145 (2019).
[26] R. Farhadifar, J.-C. Röper, B. Aigouy, S. Eaton, and F. Jülicher, Curr. Biol. **17**, 2095 (2007).
[27] N. S. Houssin, J. B. Martin, V. Coppola, S. O. Yoon, and T. F. Plageman, Dev. Biol. **462**, 36 (2020).
[28] E. Paluch and C.-P. Heisenberg, Curr. Biol. **19**, R790 (2009).
[29] D. A. Fletcher and R. D. Mullins, Nature (London) **463**, 485 (2010).
[30] A. Munjal and T. Lecuit, Development **141**, 1789 (2014).
[31] C.-P. Heisenberg and Y. Bellaïche, Cell **153**, 948 (2013).
[32] A. Shellard and R. Mayor, J. Cell Sci. **132**, jcs226142 (2019).
[33] K. Röper, BioArchitecture **3**, 45 (2013).
[34] D. N. Clarke and A. C. Martin, Curr. Biol. **31**, R667 (2021).
[35] G. A. Stooke-Vaughan and O. Campàs, Curr. Opin. Genet. Dev. **51**, 111 (2018).